## **PROCEEDINGS OF SPIE**

SPIEDigitalLibrary.org/conference-proceedings-of-spie

# Standardization of fluorescence molecular imaging systems

Dimitris Gorpas
Maximilian Koch
Maria Anastasopoulou
Uwe Klemm
Vasilis Ntziachristos



### **Standardization of Fluorescence Molecular Imaging Systems**

Dimitris Gorpas<sup>a,b</sup>, Maximilian Koch<sup>a,b</sup>, Maria Anastasopoulou<sup>a,b</sup>, Uwe Klemm<sup>a</sup>, Vasilis Ntziachristos<sup>a,b,\*</sup>

<sup>a</sup>Helmholtz Zentrum München, Institute for Biological and Medical Imaging, Ingolstädter
Landstrasse 1, Neuherberg D-85764, Germany

<sup>b</sup>Technical University Munich, Chair for Biological Imaging, Arcisstrasse 21, Munich D-80333,

Germany

#### **ABSTRACT**

Lack of standardization in fluorescence imaging challenges its clinical translation. We investigate the use of a composite phantom to perform standardization, which could serve as a framework toward the benchmarking of fluorescence imaging systems.

Keywords: Standardization, fluorescence molecular imaging, imaging systems benchmarking

#### 1. INTRODUCTION

Fluorescence imaging has proven potential to improve surgical guidance and thus positively impact the clinical management and prognosis of numerous diseases. Nevertheless, a critical issue associated with the clinical translation of this technology is related to the reproducibility of the collected measurements. Images acquired from the same fluorescent target using different cameras may vary considerably when the employed systems present markedly different specifications.

Therefore, methods for standardizing fluorescence imaging is an unmet need for assessing the performance of various systems and agents and for providing a reference to the recorded data <sup>1</sup>. During the last few years there has been proposed a number of phantoms targeting the comparison and/or validation of fluorescence imaging systems <sup>2, 3</sup>. Most of these phantoms, however, resolve one or a few parameters and provide a limited characterization of the variables associated with fluorescence imaging performance.

Recently we proposed a composite phantom that integrates multiple targets within the field of view of a fluorescence camera <sup>4</sup>. In the work presented herein we sought to introduce a methodology that has the potential to standardize fluorescence cameras through a single or a few image acquisitions of the phantom. We show, for the first time, how composite phantoms can be employed for comparing systems of different specifications. The described benchmarking method may become critical for standardization of imaging systems with broader applications for clinical translation of fluorescence molecular imaging.

#### 2. MATERIALS AND METHODS

Each quadrant of the phantom employed in this study resolves different fluorescence features, as described in our previous study <sup>4</sup>: (1) sensitivity as a function of the optical properties; (2) sensitivity as a function of the depth from the top surface; (3) resolution of the fluorescence and optical imaging; and (4) cross-talk from the excitation light. In addition, there exist five wells at the corners and center of the phantom for assessing field illumination (i.e., the source for reflectance color imaging) homogeneity.

In order to test our main hypothesis, that is standardization of fluorescence imaging systems is feasible through imaging a composite phantom, we used two systems of different specifications. The first system (C-1) is described in details elsewhere 5. Briefly, C-1 employs a 750 nm CW laser diode (BWF2-750-0, B&W Tek, Newark, Delaware, United States)

Novel Biophotonics Techniques and Applications IV, edited by Arjen Amelink, I. Alex Vitkin, Proc. of SPIE-OSA Vol. 10413, 104130J · © 2017 OSA-SPIE CCC code: 1605-7422/17/\$18 · doi: 10.1117/12.2286065

Proc. of SPIE-OSA Vol. 10413 104130J-1

<sup>\*</sup> v.ntziachristos@tum.de; phone: +49 (0) 89 3187 3852; https://www.helmholtz-muenchen.de/ibmi/index.html

for excitation, while detection is spectrally resolved in two channels by a dichroic mirror (700DCXXR, AHF analysentechnik AG, Tubingen, Germany). The emitted fluorescence is transmitted through the first channel and after filtered by a NIR filter (ET810/90, Chroma Technology) is recorded by an iXon electron multiplying charge-coupled device (EMCCD, DV897DCS-BV, Andor Technology, Belfast, Northern Ireland). Reflectance color imaging is enabled by the second channel, which is within the spectral range 450 to 700 nm, and a 12-bit color charge-coupled device (CCD) camera (pixelfly qe, PCO AG, Kelheim, Germany). The second system (C-2) also employs an EMCCD camera (Luca R, Andor Technology) for fluorescence detection, however presents significantly lower quantum efficiency than the EMCCD of C-1 (i.e. ~70% of C-1 vs ~40% of C-2 at 800 nm) and the detection band is centered at 850 nm (D850/40 m, Chroma Technology), instead of the 810 nm of C-1. In addition, C-2 lacks the reflectance color imaging channel.

Automated extraction of all phantom components was implemented through application of the speeded-up robust features (SURF) algorithm. Two templates were designed, one for the fluorescence images of the phantom (Fig. 1a) and one for the reflectance images (Fig. 1c). Reflectance images were acquired either through the two EMCCDs with the room lights turned on or through the CCD of C-1. The application of the SURF algorithm provides the geometric transformation to project the template onto the acquired images, and thus enables the extraction of all phantom components. This allows for the quantification of the camera performance metrics, i.e., magnification, optical resolution, diffused fluorescence resolution, excitation light leakage and parasitic illumination, sensitivity and field illumination homogeneity, without any user interference.

Specifically: (1) Magnification is approximated by the ratio of the phantom's width versus the Euclidean distance in Cartesian coordinates between two adjacent corners of the phantom on the imaging plane. (2) The definition of the optical resolution is based on the standard 1951 United States Air Force resolution test chart (USAF-1951) and the estimation of the contrast transfer function (CTF) as expressed by the Michelson's formula:

$$CTF_{i} = \frac{\max(I_{i}) - \min(I_{i})}{\max(I_{i}) + \min(I_{i})}$$
(1)

where  $I_i$  denotes the per pixel intensity values for each one of the USAF-1951 target's elements. Adopting the Rayleigh criterion for optical imaging, the limit where CTF is ~26.4% defines the USAF-1951 target's elements that can be fully resolved by the system. (3) The L-shaped element of the phantom (Fig. 1a) is employed for the estimation of the diffused fluorescence resolution. The CTF is employed, as in optical resolution, for the approximation of the diffused fluorescence resolution and is calculated over every line segment that is perpendicular to the bisector of the L-shaped element. The line segment over the CTF threshold of ~26.4% that is closer to the concave corner of the element describes the diffused fluorescence resolution of the investigated system. (4) The upper left quadrant of the phantom consists of a highly absorbing and a highly scattering well. Those two are employed for the approximation of the excitation light leakage and the parasitic illumination. In the first case, the light leakage is estimated through the transmission ratio between the average pixel intensity of the highly scattering element to that of the highly absorbing element in the fluorescence images. On the other hand, the equivalent transmission ratio is estimated in the dark images for the approximation of the parasitic illumination. For both ratios, a value equal or smaller than 1 implies reduced contamination of the fluorescence images. (5) Sensitivity is assessed by the signal to noise ratio (SNR) expressed as  $SNR_{dR} = 20 \cdot \log(S/RMSN)$ , where S is the average intensity within each well of the two right quadrants of the phantom (Fig. 1a). The top right quadrant describes the sensitivity as a function of the optical properties, while the bottom right one describes the sensitivity as a function of the depth. **RMSN** is the root mean square noise derived by the phantom's main body. (6) The homogeneity of the field illumination can be approximated using the five highly scattering elements located at the four corners and the center of the phantom. Flat-fielding can be achieved by applying bicubic splines interpolation of the average intensity from each of the five elements and dividing the acquired reflectance images with the resulting profile.

The primary hypothesis of the study described herein is that benchmarking of fluorescence imaging systems is feasible through imaging of the composite phantom. To test this hypothesis, we employed two systems of markedly different specifications (C-1 and C-2). The acquisition settings of C-1 were fixed (i.e. working distance at 320 mm, gain at 4000, no pixel binning), while C-2 acquired data from two different working distances (i.e. 320 mm and 200 mm) and for variable pixel binning settings  $(1 \times, 2 \times, \text{ and } 4 \times)$ . The gain of C-2 was adjusted accordingly to avoid saturation. For all tests implemented the exposure time was 0.1 sec to resemble actual intraoperative applications.

#### 3. RESULTS AND DISCUSSION

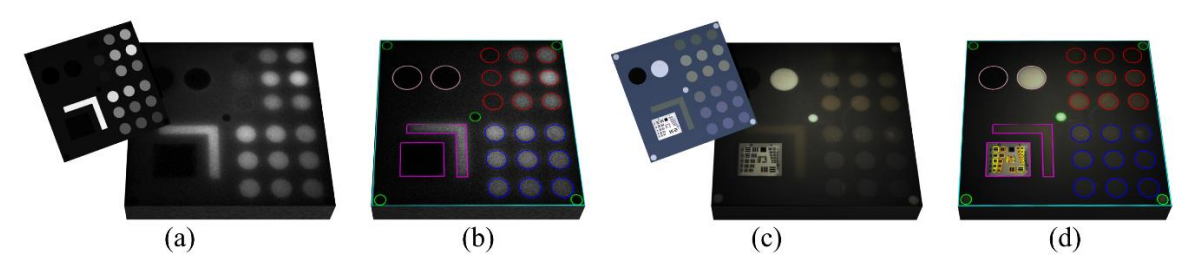


Figure 1. The process for extracting the phantom elements. (a) A fluorescence image acquired by C-1 and the corresponding template. (b) The phantom elements delineated on the fluorescence image after the application of the SURF algorithm. Each color describes the corresponding quadrant of the phantom. (c) A reflectance image acquired by C-1 and the corresponding template. (d) The phantom elements delineated on the fluorescence image after the application of the SURF algorithm. Each color describes the corresponding quadrant of the phantom.

Figure 1 shows the fluorescence and reflectance image pair acquired by C-1, as well as the registration between the acquired images and the templates. Specifically, Fig. 1a shows the fluorescence image from C-1, while in top left is shown the corresponding template used by the SURF algorithm. After the estimation of the geometric transformation all phantom components are extracted. Figure 1b depicts the fluorescence image with the boundaries of all phantom elements color-coded according to the quadrant they belong. Similarly, Fig. 1c shows the reflectance color image from C-1, along with the corresponding template at the top left. The result of the template matching process is shown in Fig. 1d. The fluorescence image shown in Fig. 1b is employed for the determination of the fluorescence performance parameters of the two cameras for the various experimental configurations (i.e., fluorescence resolution, excitation light leakage, parasitic illumination, and sensitivity), while the reflectance image is used for the determination of the optical parameters (i.e., optical resolution, magnification).

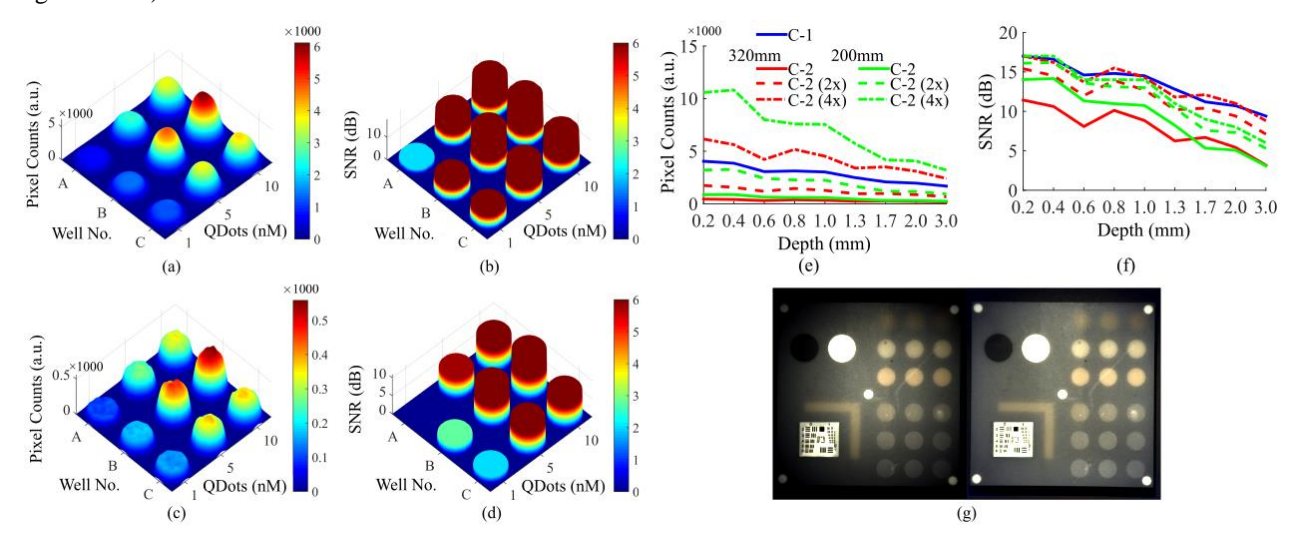


Figure 2. Representative results from the standardization process. (a) The pixel counts from the top right quadrant of the phantom (Fig. 1) as acquired by C-1. (b) The corresponding SNR values, thresholded at 6dB. (c)-(d) The corresponding results from C-2 at 320 mm working distance without pixel binning. (e) The pixel counts as a function of depth (bottom right quadrant) for all experimental configurations. (f) The corresponding SNR values. (g) Correction for illumination homogeneity through flat-fielding; left: uncorrected reflectance image acquired by the CCD of C-1; right: the corrected reflectance image.

Figure 2 depicts some representative results of the comparison between the different experimental configurations. The pixel counts and the SNR from C-1 of the 9 wells with different optical properties are shown in Figs. 2a and 2b. The SNR has been thresholded at 6 dB, which correspond to the critical value for a 95% confidence of normal signal distributions. The saturated part of the cylinders represents the distance of the SNR value at each specific well from that threshold. The corresponding results, as derived by C-2 at the same working distance as C-1 and without any pixel binning, are shown in

Figs. 2c and 2d. As expected from the narrower spectral band of C-2 and the lower quantum efficiency of the camera, compared to C-1, both pixel counts and SNR are much smaller than those from C-1. Results from the 9 wells of different depth (lower right quadrant) are shown in Figs. 1e and 1f, for all experimental configurations tested. From these panels it becomes apparent that changes in the acquisition settings of a camera system affect the recorded data. This fact is the basis of the proposed benchmarking process. Specifically, the automated method of analyzing the acquired data allows for objective determination of the acquisition parameters that could lead to equivalent results from two markedly different imaging systems. Adopting a least squares method between all metrics quantified through the phantom, it derived that C-2 with working distance of 200 mm and 2× pixel binning is the configuration that approaches better the performance of C-1.

An additional feature of the employed phantom is the possibility to perform flat-fielding in the acquired reflectance images through the 5 highly scattering wells at the corners and center of the phantom. Figure 2g shows a representative result of this process, where the average intensity of those wells in the left image was employed to approximate the illumination profile through bicubic splines interpolation. This profile was then used to normalize the acquired reflectance image, leading to the right image of Fig. 2g. Intensity distribution is now considerably more uniform, without any influence on the color of the acquired image.

#### 4. CONCLUSION

The study described herein represents an attempt of standardizing fluorescence imaging systems with a composite phantom. Overall, we expect that the field of standardization will play a major role in the growth of fluorescence molecular imaging.

#### **REFERENCES**

- [1] V. Ntziachristos, and D. Hyde, "In-vivo Fluorescence Imaging: Applications, Future Trends & Approaches to Standardization," in Standardization and Quality Assurance in Fluorescence Measurements II: Bioanalytical and Biomedical Applications U. Resch-Genger, Ed., pp. 549-560, Springer Berlin Heidelberg, Berlin, Heidelberg (2008).
- [2] B. Zhu et al., "Validating the Sensitivity and Performance of Near-Infrared Fluorescence Imaging and Tomography Devices Using a Novel Solid Phantom and Measurement Approach," Technol. Cancer. Res. Treat. 11(1), 95-104 (2012).
- [3] B. W. Pogue, and M. S. Patterson, "Review of tissue simulating phantoms for optical spectroscopy, imaging and dosimetry," J. Biomed. Opt. 11(4), 041102 (2006).
- [4] M. Anastasopoulou et al., "Comprehensive phantom for interventional fluorescence molecular imaging," J. Biomed. Opt. 21(9), 091309 (2016).
- [5] J. Glatz et al., "Concurrent video-rate color and near-infrared fluorescence laparoscopy," J. Biomed. Opt. 18(10), 101302 (2013).